

# Nanoscale functionalization of MoS<sub>2</sub> monolayers with DNA origami

*Shen Zhao<sup>1,2</sup>, Zhijie Li<sup>1,3</sup>, Zsófia Meggyesi<sup>1</sup>, Elisabeth Erber<sup>1</sup>, Christoph Sikeler<sup>1</sup>, Kenji Watanabe<sup>4</sup>, Takashi Taniguchi<sup>5</sup>, Anvar S. Baimuratov<sup>1,2,6\*</sup>, Tim Liedl<sup>1\*</sup>, Alexander Högele<sup>1,2</sup>, and Irina V. Martynenko<sup>1,6\*</sup>*

<sup>1</sup>Faculty of Physics and Center for NanoScience (CeNS),

Ludwig-Maximilians-Universität München

Geschwister-Scholl-Platz 1, 80539 Munich, Germany,

<sup>2</sup>Munich Center for Quantum Science and Technology (MCQST),

Schellingstraße 4, 80799 München, Germany

<sup>3</sup>Institute of Physics, Carl von Ossietzky University, 26129

Oldenburg, Germany

<sup>4</sup>Research Center for Electronic and Optical Materials, National Institute for Materials Science, 1-1 Namiki, Tsukuba 305-0044, Japan

<sup>5</sup>Research Center for Materials Nanoarchitectonics, National Institute for Materials Science, 1-1 Namiki, Tsukuba 305-0044, Japan

<sup>6</sup>Skolkovo Institute of Science and Technology, Moscow 121205, Russia

Corresponding authors:

Anvar S. Baimuratov [anvar.baimuratov@physik.uni-muenchen.de](mailto:anvar.baimuratov@physik.uni-muenchen.de)

Tim Liedl [tim.liedl@physik.lmu.de](mailto:tim.liedl@physik.lmu.de)

Irina V. Martynenko [irina.martynenko@physik.uni-muenchen.de](mailto:irina.martynenko@physik.uni-muenchen.de)

The functionalization of two-dimensional (2D) materials with organic molecules is a promising approach for realizing nanoscale optoelectronic devices with tailored functionalities, such as quantum light generation and *p-n* junctions. However, achieving control over the molecules' precise positioning on the 2D material remains a significant challenge. Here, we overcome the limitations of solution- and vapor deposition methods and use a DNA origami placement technique to spatially arrange various organic molecules on a chip surface at the single-molecule level with high assembly yields. This versatile method allows for precise patterning of transition metal dichalcogenides (TMDs) with organic molecules, including thiols and fluorescent dyes. We successfully integrated MoS<sub>2</sub> monolayers with micron-scale molecule-origami patterns achieving both single photon emission from thiol-induced localized excitons in MoS<sub>2</sub> and photoexcitation energy transfer with patterned fluorescent dyes. Our approach offers a pathway for producing complex,

tailored 2D inorganic-organic heterostructures with molecular-level control, opening up new possibilities for advanced materials and device design.

Combining inorganic atomically-thin semiconductors such as TMD<sup>1, 2</sup> with organic molecules, novel device architectures can be designed as high-performance photodetectors,<sup>3,4</sup> *p-n* junctions,<sup>5, 6, 7</sup> chemical sensors,<sup>8</sup> and catalytic systems.<sup>9</sup> In these devices, organic molecules deposited on the surface of TMDs introduce charge doping<sup>10</sup> or energy-transfer states<sup>11</sup>, leading to changes in their optical,<sup>12</sup> electronic, thermoelectric,<sup>13</sup> and magnetic properties.<sup>14</sup> Assembling such hybrid devices at the molecular scale involves a number of challenging requirements, including nanometer-precise control of molecule pattern, scalability and versatility in the choice of molecule. Current fabrication methods offer limited control over the homogeneity and positioning of organic molecules and the stability of the final hybrid structure, which hampers progress in this field.

Chemical doping methods such as chemical surface functionalization via the non-covalent<sup>15</sup> or covalent<sup>16</sup> bonding of adsorbed molecules are commonly used to fabricate hybrid structures. However, solution processing methods such as spin-coating, drop-casting, or vapor-based methods lack full control over molecule concentration and position on a 2D material surface. Conventional photolithography processes that are used to pattern layers of organic molecules on top of 2D materials including photochemical reactions, chemical etching or laser writing<sup>17, 18, 19</sup> can damage atomically thin materials. While molecular self-assembly approaches<sup>20, 21, 22</sup> can create atomically precise arrays of molecules on 2D materials like graphene,<sup>23</sup> these methods are often molecule-specific and lack the flexibility to design arbitrary patterns of molecules.

Structural DNA nanotechnology, particularly DNA origami self-assembly<sup>24, 25</sup>, enables bottom-up fabrication of highly defined, complex two- and three-dimensional nanostructures with single-nanometer resolution.<sup>26, 27, 28, 29, 30, 31, 32</sup> DNA origami is widely used as a molecular scaffold, enabling sub-nanometer precision in positioning molecules and nanoparticles.<sup>33, 34, 35, 36, 37, 38</sup> Kershner et al. developed a DNA origami placement (DOP) technique by combining DNA origami self-assembly with lithographic nanopatterning, enabling the site- and shape-selective deposition of individual DNA origami objects into arrays on patterned substrates.<sup>39</sup> DOP overcomes the limitations of top-down lithography and gives access to high-yield placement and arrangement of individual nanoscale components such as metallic nanoparticles<sup>40, 41, 42</sup> and organic dyes<sup>43, 44</sup> into precise arrays and patterns. Progressing from these achievements, an approach that allows the fabrication of molecular patterns for TMD functionalization with high spatial precision is highly desirable.

Here, we demonstrate programmable 2D material – organic molecule hybrids with high efficiency and spatial precision. By dry-stamp transferring micron-scale chemical-vapour-deposited MoS<sub>2</sub> monolayers onto the chips patterned with DNA origami triangles bearing either 54 thiol molecules or fluorescent dyes, we rationally design hybrid systems with two distinct functionalities: either localized in-gap states or photoexcitation energy transfer between the fluorescent dyes and MoS<sub>2</sub>. Cryogenic PL of thiol-origami-MoS<sub>2</sub> exhibit  $g^{(2)}(0)$  values below 0.5, confirming single-photon emission from thiol-induced localized states in MoS<sub>2</sub>. We achieve an ~ 90% yield of single-photon emitter placement. Our method provides a powerful platform for precise engineering the properties of 2D materials at the nanoscale and opens the path for producing miniaturized hybrid inorganic/organic devices with increased device performance.

## Fabrication design

DNA origami triangles with 127-nm long outer edges were used as “molecular adaptors” to precisely position various organic molecules on micron-scale patterns on a chip via the DNA origami placement technique (Fig. 1a). A TMD monolayer was subsequently transferred on top of the molecule-origami pattern resulting in the exciton localization or energy transfer between TMD and molecules (Fig. 1b). The various steps of the fabrication process are illustrated in Fig. 1c. First, DNA triangles, designed *in-silico*<sup>45, 46</sup> and folded in buffer containing MgCl<sub>2</sub> (Fig. 1d) were deposited onto specific binding sites that were created via electron-beam (e-beam) patterning of negatively charged hydroxyl groups (green, hydrophilic; water contact angle < 10°) within a background of hydrophobic methyl groups (pink, hydrophobic; water contact angle ≈ 75°) on a Si/SiO<sub>2</sub> substrate. Negatively charged origami (grey) binds strongly to the charged spots via positively charged Mg<sup>2+</sup> ions from buffer solution while the hydrophobic, thus passivated area, binds origami poorly.

To prepare the substrates and place the DNA origami, we followed protocols reported in detail before.<sup>42, 47</sup> Briefly, we incubated a solution of purified DNA triangles in a buffer containing MgCl<sub>2</sub> over the patterned chips, resulting in a high yield (more than 90%) of single origami binding events<sup>42</sup> (Fig. 1e). Every DNA triangle carries 54 3'-adenine “anchor” strands, each 21 nt long, extending from the triangle every 12 nanometers along both its inner and outer edges, as schematically depicted in Fig. 1a (the design of the anchor strand is presented in Supplementary Note 1 and Supplementary Fig. 1). Next, surface-bound DNA triangles were functionalized with organic molecules by annealing to the anchor strands 19 nt thymine strands bearing on their 5' ends either a single thiol group or a fluorescent dye molecule (ATTO633 or ATTORho101).

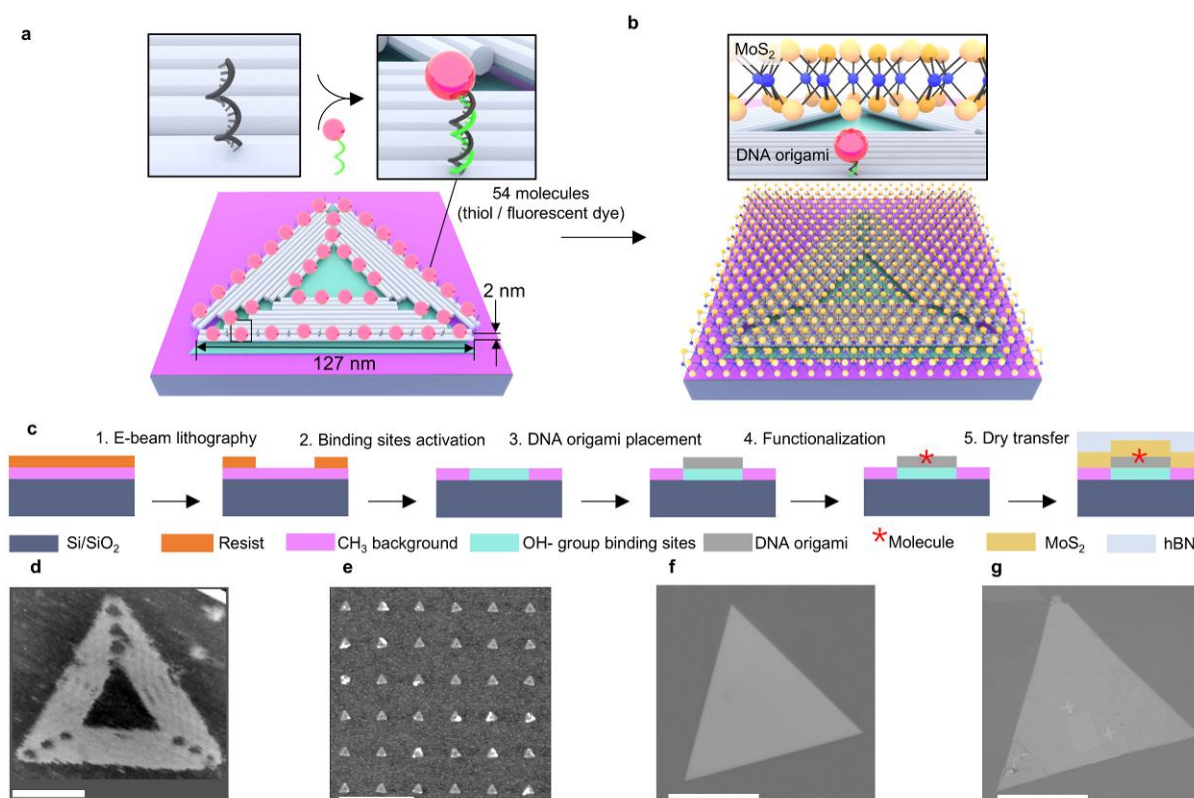


**Figure 1. DNA origami-programmable organic molecule-MoS<sub>2</sub> hybrid assembly.** (a) Schematic illustration of a DNA origami triangle positioned on a hydrophilic, hydroxyl group covered binding site (green) on a hydrophobic, methyl group covered surface of Si/SiO<sub>2</sub> chip. DNA origami triangle bears 54 adenine “anchor” strands each 21 nt long for on-surface annealing with 19 nt thymine strands bearing a single functional molecule. (b) Schematic illustration of a molecule-origami-MoS<sub>2</sub> assembly. (c) The various steps of the fabrication process of a molecule-origami-MoS<sub>2</sub> assembly. (d) Liquid mode AFM image of DNA origami

triangle in the folding buffer. (e) AFM image of a dried Si/SiO<sub>2</sub> chip with the DNA origami triangles positioned onto ~120 nm triangular binding sites in a 20 μm-square array with a 250 nm period, fabricated using electron beam lithography. (f) Bright-field microscopy image of the MoS<sub>2</sub> flake on adhesive polycarbonate stamp before transferring onto an origami pattern. (g) Bright-field microscopy image of the MoS<sub>2</sub> flake transferred onto the origami pattern. The scale bar in panel (d) is 50 nm, in panel (e) is 500 nm, and in panels (f) and (g) is 30 μm.

After the placement and functionalization, the Si/SiO<sub>2</sub> chips with molecule-origami patterns were air-dried. Atomic force microscopy (AFM) measurements of dried patterns reveal the typical height of DNA triangles of 2 nm, consistent with the height of a DNA duplex (Fig. 1e; a detailed description of every DNA pattern design used in this study, along with AFM characterization and height profiles of the air-dried molecule-origami patterns, is presented in Supplementary Note 2, Supplementary Figs. 2–4.). Finally, triangular single-crystal monolayers of MoS<sub>2</sub> covered by hexagonal boron nitride (h-BN) flakes (Fig. 1f) were transferred on top of a molecule-origami pattern by using an adhesive polycarbonate (PC) stamp. Fig. 1g depicts a representative optical microscope image of the resulting hybrid assemblies with the origami pattern being fully covered with MoS<sub>2</sub>.

### Precise functionalization with thiol derivative molecule

Covalent functionalization of monolayer MoS<sub>2</sub> using thiol derivative molecules is a widely employed and convenient approach for modulating its electronic properties.<sup>48</sup> Numerous studies have demonstrated that once thiols are attached to MoS<sub>2</sub> via a conjugation reaction, the terminal groups of the molecules act as dopants and alter the material's carrier density through electron-donating (*n*-doping) or electron-withdrawing (*p*-doping) mechanisms.<sup>49, 50</sup> Thiol groups form robust bonds with MoS<sub>2</sub>, ensuring stability of the hybrid structures, and the readily available thiol-modified oligonucleotides offer a pathway for precise positioning of individual thiol derivatives on a surface using the DOP method.

We fabricated Si/SiO<sub>2</sub> chips containing 25 μm × 25 μm square arrays of DNA origami triangles with 170 nm periods (Supplementary Fig. 2 shows the pattern design and AFM characterization). Surface-bound triangles were functionalized with 19 nt thymine strands, each bearing a single thiol group attached to the phosphate group of the terminal thymine via a six-carbon atom spacer. Next, we transferred the MoS<sub>2</sub> flake on top of the thiol-origami pattern and annealed the sample under ultrahigh vacuum for 12 hours.

We recorded room-temperature (RT) photoluminescence (PL) maps of MoS<sub>2</sub> transferred onto thiol-origami patterns and non-thiolated origami references. Both non-patterned MoS<sub>2</sub> and MoS<sub>2</sub> deposited on non-thiolated patterns exhibit similar PL spectra, characteristic of MoS<sub>2</sub> monolayers on dielectric substrates (see Supplementary Note 3 and Supplementary Fig. 5). Namely, PL spectra contain a single peak at 1.88 eV, corresponding to the lowest excitonic resonance, known as the A exciton.<sup>51</sup> This exciton corresponds to the momentum-direct transition at the K-valleys in the Brillouin zone of the MoS<sub>2</sub> monolayer.

However, MoS<sub>2</sub> regions patterned with thiol-origami consistently exhibit quenching of the MoS<sub>2</sub> exciton peak at 1.88 eV and the appearance of a red-shifted peak at 1.83 eV in the PL spectra (Supplementary Fig. 5). This suggests that the thiol-origami is responsible for the observed PL modulation. Notably, the red-shifted peak is not attributable to trion states, as the monolayer MoS<sub>2</sub> trion binding energy 34 meV<sup>52, 53</sup> is less than the observed 50 meV energy splitting between the A exciton and the red-shifted peak. This splitting is more consistent with localized exciton states, such as those created by helium ion irradiation.<sup>54</sup> We hypothesize that thiol-origami binding to MoS<sub>2</sub> results in the formation of localized in-gap defect states. Excitons with energies of 1.88 eV and 1.83 eV will be referred to as free and localized excitons, respectively.

To demonstrate the excellent control over localized exciton density afforded by our DNA origami-based functionalization strategy, we fabricated thiol-origami square arrays with periods increasing gradiently from 170 nm to 1000 nm (Fig. 2a; see Supplementary Fig. 3 for AFM characterization). PL maps of free and localized excitons are shown in Figs. 2b and 2c, respectively. The highest-density pattern with 170 nm period exhibits near-complete quenching of free exciton PL and strong localized exciton PL. As the period increases, a stepwise increase in free exciton PL is observed, accompanied by a corresponding decrease in localized exciton PL (Fig. 2d), confirming the efficiency of our approach.

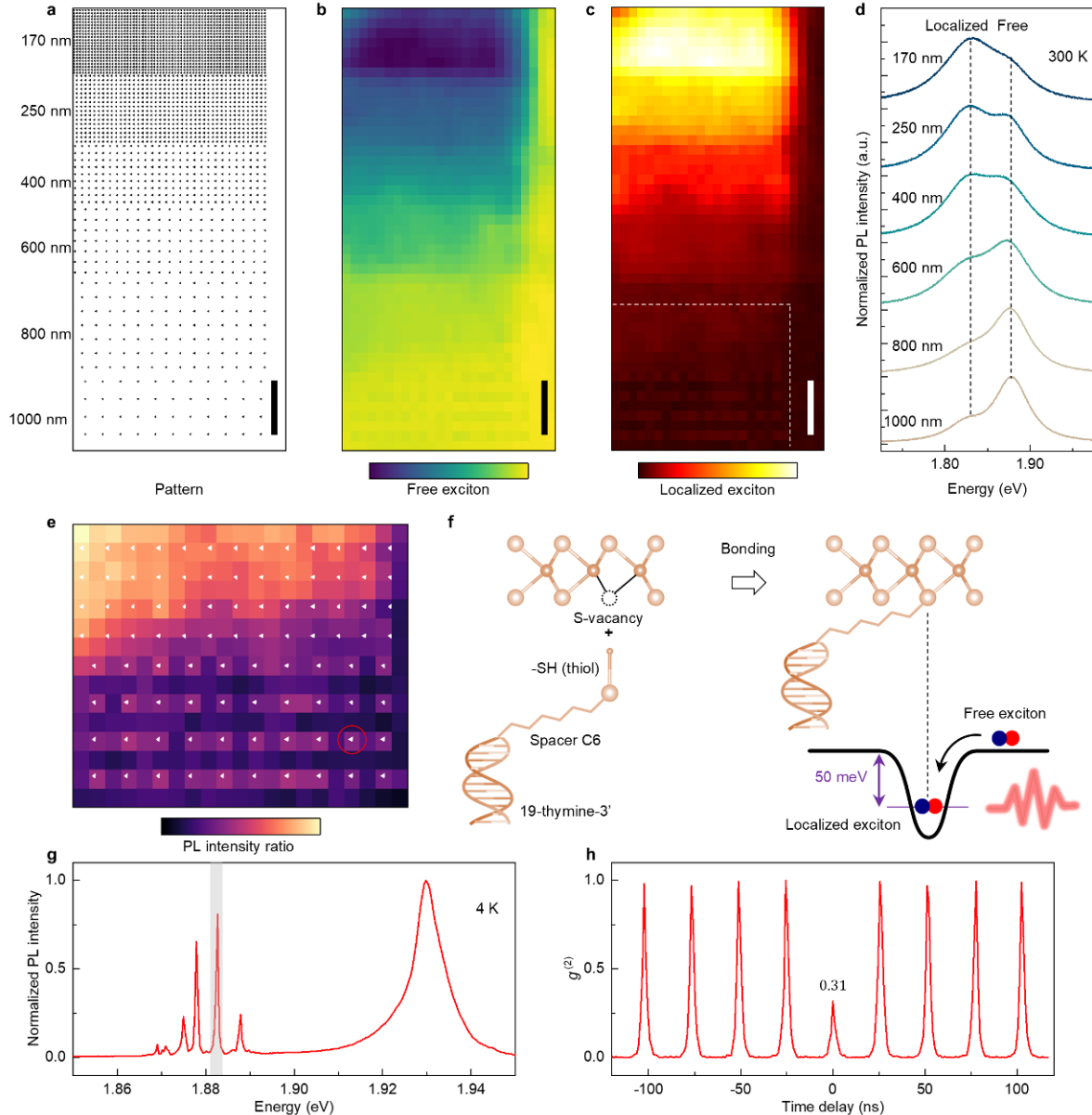


**Figure 2. DNA-programmable exciton landscape in MoS<sub>2</sub> flake on top of the thiol-origami pattern.** (a) Schematic of the patterned area. The nanopatterned area is 20  $\mu\text{m}$  x 25  $\mu\text{m}$  and consists of arrays of triangular binding sites with a size of 120 nm in a square lattice with periods ranging from 1000 nm to 170 nm. (b, c) Free exciton and localized exciton PL intensity maps, measured at 1.88 eV and 1.83 eV, respectively. (d) Representative room-temperature PL spectra of every "step" in the gradient pattern presented in Fig. 2a. (e) Map of localized/free exciton PL peaks ratio, corresponding to the marked area in panel c. Each white triangle indicates the position of a DNA origami triangle. (f) Schematic illustration of the exciton localization scheme in thiol-origami-MoS<sub>2</sub>. (g) Low-temperature PL spectrum from the spot indicated by the red circle in panel (e). (h) Correlation function of localized defect state marked by gray bar in panel (g) with second order coherence at zero time delay  $g^{(2)}(0)=0.31$ . Scale bars: 4  $\mu\text{m}$  (panels a, b, and c).

Due to the diffraction-limited optical resolution of  $\sim 1 \mu\text{m}$ , we could not spatially resolve PL signals from individual lattice sites when the thiol-origami periods ranged from 170 to 800 nm; instead, we observed relatively homogeneous PL signals in these regions. However, at a pattern period of 1000 nm, we were able to optically resolve PL signal variations corresponding directly to the positions of individual thiol-origami. Fig. 3e depicts the ratio of PL intensities for the localized and free exciton peaks. Localized exciton PL is enhanced at all lattice sites compared to the inter-lattice regions. This indicates efficient thiol group binding to MoS<sub>2</sub> and formation of localized defects within the MoS<sub>2</sub> electronic structure. We attribute the binding to a chemisorption of thiols to sulfur vacancies in MoS<sub>2</sub> as illustrated in Fig. 2f. Despite the limited number of vacancy sites of  $\sim 10^{13} \text{ cm}^{-2}$  in MoS<sub>2</sub>,<sup>55</sup> the high density of these sites compared to our thiolated strands (estimated at  $\sim 10^{12} \text{ cm}^{-2}$ , with each DNA triangle carrying 54 thiolated strands) ensures efficient binding. Thiol-MoS<sub>2</sub> binding sites are forming trapping potentials for exciton complexes, resulting in emission at an energy 50 meV lower than the free exciton in MoS<sub>2</sub>.

Single-photon sources are a key application of exciton localization in TMDs.<sup>56, 57, 58, 59, 60</sup> We performed cryogenic optical spectroscopy at 4 K on thiol-origami-MoS<sub>2</sub> pattern with a 1000 nm period. Fig. 2g shows a typical PL spectrum from individual thiol-origami site marked by the red circle in the Fig. 2e. At low temperature, both free and localized MoS<sub>2</sub> emission peaks are blue shifted by  $\sim 50 \text{ meV}$ .<sup>61, 62</sup> The broad PL of localized excitons resolves into several sharp peaks, each with a linewidth below 1 meV. Fig. 2h presents the second-order photon-correlation function  $g^{(2)}(\tau)$  for a single sharp peak (marked in grey in Fig. 2g). The measured  $g^{(2)}(0)$  value of 0.31, well below the 0.5 threshold, demonstrates single-photon emission from our thiol-origami patterned MoS<sub>2</sub>. A residual multiphoton emission is observed due to the use of 54 thiolated strands per origami, resulting in multiple individually generated localized states. The efficient binding is validated by a 0.88 yield of single-photon emitter placement, as 29 out of 33 measured thiol-origami sites exhibited single-photon emission peaks (see Supplementary Fig. 6 for PL data and statistical analysis). These results highlight DNA origami as a unique and versatile tool for customizing MoS<sub>2</sub> materials with precisely targeted localized defects including single-photon emitters. Further tuning the number of thiol molecules per origami and exploring different organic molecules provides a route to improve single-photon purity<sup>63</sup> and generate chiral quantum light.<sup>64</sup>

### Photoexcitation energy transfer patterning

The use of MoS<sub>2</sub> in nanophotonic devices such as LEDs, lasers, and optical networks is hindered by its low PL quantum yield.<sup>12</sup> Recent respective approaches to enhance emission intensity of MoS<sub>2</sub> is through nonradiative energy transfer, where excitation energy is transferred from a donor to a MoS<sub>2</sub> acceptor.<sup>65</sup>

We apply our nanofabrication method to locally enhance MoS<sub>2</sub> PL by using Förster resonance energy transfer (FRET). In general, FRET occurs when there is a spectral overlap between the PL spectrum of the donor and absorption spectrum of the acceptor.<sup>66</sup> FRET efficiency between a 0D fluorescent dye dipole and 2D materials like MoS<sub>2</sub> is proportional to  $z^{-4}$ , where  $z$  is the distance between the 0D and 2D structures.<sup>67, 68</sup>

To fulfill the FRET conditions, we use fluorescent ATTO633 dye with a PL band position overlapping well with the lowest exciton band (A exciton) of the MoS<sub>2</sub>. Fig. 3a displays the room temperature absorption and PL spectra of monolayer MoS<sub>2</sub>, along with the PL and absorption spectra of the ATTO633 dye in PBS. The characteristic MoS<sub>2</sub> absorption and PL bands of the A exciton are located at 1.89 eV and 1.88 eV, respectively. The dye's PL spectrum efficiently overlaps with the MoS<sub>2</sub> absorption. The energy of fundamental transition

$S_0$ - $S_1$  in ATTO633 dye is approximately 1.93 eV, slightly larger than 1.88 eV of  $\text{MoS}_2$ , prohibiting reverse energy transfer from  $\text{MoS}_2$  to the dye.<sup>67</sup>

To implement FRET in a ATTO633-origami- $\text{MoS}_2$  hybrid assembly, we fabricated Si/SiO<sub>2</sub> chips with 40  $\mu\text{m}$ -sized continuous fractal triangle filling curves with 1  $\mu\text{m}$  line thickness. Multiple origamis bind at random positions and orientations within these curves, forming a dense, single layer of origami (Supplementary Fig. 4 depicts the pattern design and AFM characterization). After on-surface functionalization of the origami with 19 nt thymine strands bearing single ATTO633 dye molecules, we then transferred a  $\text{MoS}_2$  flake onto the ATTO633-origami pattern, ensuring complete coverage (Fig. 3b).

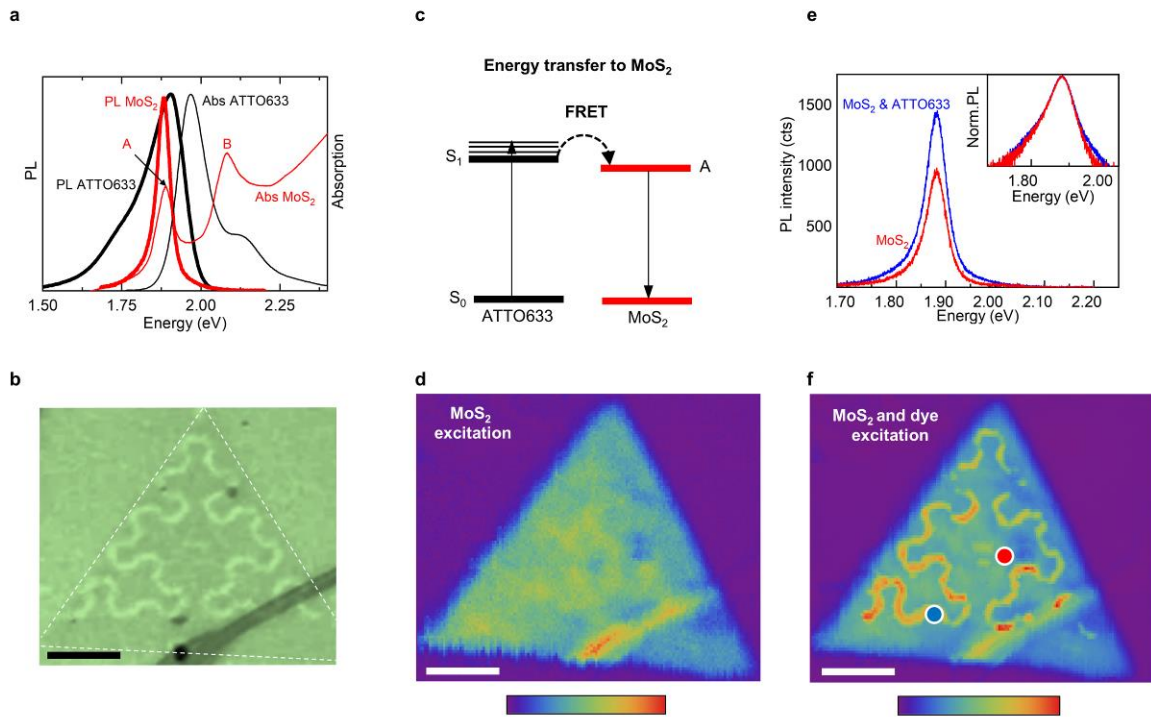


**Figure 3. DNA-programmable enhancement of PL of  $\text{MoS}_2$ .** (a) Room-temperature absorption (thin lines) and PL spectra (thick lines) of the  $\text{MoS}_2$  flake and of the ATTO633 dye in PBS. A and B indicate the  $\text{MoS}_2$  exciton bands. (b) Bright-field microscopy image of the  $\text{MoS}_2$  flake transferred on top of the ATTO633-origami pattern. (c) Schematic illustration of energy transfer scheme between ATTO633 dye and  $\text{MoS}_2$ . (d) Room-temperature PL map of the  $\text{MoS}_2$  flake on top of the ATTO633-origami pattern. PL excitation energy is 2.36 eV (525 nm) where the ATTO633 dye has negligible absorption. (e) Room-temperature PL map of the  $\text{MoS}_2$  flake on top of the ATTO633-origami pattern. PL excitation energy was 2.21 eV (560 nm) where both  $\text{MoS}_2$  and ATTO633 dye absorb light. (f) Room-temperature PL spectra of ATTO633-origami- $\text{MoS}_2$  hybrid assembly (orange curve) and  $\text{MoS}_2$  flake alone (violet curve). Inset shows the corresponding normalized PL spectra. Scale bars in (b), (d) and (f) are 10  $\mu\text{m}$ .

We assume that upon excitation of the dye by light, the photoexcitation energy is non-radiatively transferred from the dye's first excited state to the exciton states of  $\text{MoS}_2$  and then further emitted from the A exciton of  $\text{MoS}_2$  (Fig. 3c). To investigate the energy transfer in ATTO633-origami- $\text{MoS}_2$  hybrid assembly, we employed two excitation schemes: direct excitation of  $\text{MoS}_2$  at 2.36 eV, where ATTO633 dye absorption is minimal, and indirect excitation of  $\text{MoS}_2$  through the ATTO633 dye at 2.21 eV where both  $\text{MoS}_2$  and the dye absorb. Direct excitation exhibits relatively homogeneous PL across the flake, with a single exciton A peak at 1.88 eV and no local changes in PL intensity (Fig. 3d). In contrast, indirect excitation results in a significant local enhancement of  $\text{MoS}_2$  PL, revealing the ATTO633-origami pattern (Fig. 3e, f). The peak intensity of  $\text{MoS}_2$  coupled with the dye is increased by a factor of 2 compared to the non-patterned  $\text{MoS}_2$  region (Fig. 3f). We observed no signs of the broadband ATTO633 dye emission in the normalised PL spectra of the hybrid (inset of

Fig. 3e). This indicates strong quenching of the ATTO633 dye PL due to FRET. Furthermore, the absence of MoS<sub>2</sub> PL band broadening suggests that no recombination processes occur within the MoS<sub>2</sub> on the ATTO633-origami. Consequently, our patterning approach enables a two-fold local brightening of MoS<sub>2</sub> via FRET from the underlying fluorescent dye.

We further demonstrated the versatility of our technique by utilizing MoS<sub>2</sub> as a FRET donor. This was achieved using ATTO-Rho101, a dye with energy level for the fundamental transition matching a higher energy B exciton band<sup>51</sup> in MoS<sub>2</sub> at 2.1 eV (see Fig. 3a). Efficient quenching of MoS<sub>2</sub> PL confirmed energy transfer to the dye (Supplementary Note 4, Supplementary Fig. 7). This capacity for both FRET-based enhancement and quenching of MoS<sub>2</sub> PL, enabled by the selection of different fluorescent dyes, demonstrates the versatility of our method for realizing diverse functionalities.

## CONCLUSIONS

In summary, we tuned the optical and electronic properties of monolayer MoS<sub>2</sub> via coupling to the organic molecules, precisely positioned on chip surfaces using a DNA origami placement technique. After transferring the MoS<sub>2</sub> monolayer onto micron-scale thiol-origami patterns, we observed local variations in MoS<sub>2</sub>'s PL properties, attributed to exciton trapping caused by thiol-MoS<sub>2</sub> binding. Unprecedented control over density of these localized exciton was achieved by adjusting the square-lattice period of DNA pattern, allowing us to detect single-photon emission of MoS<sub>2</sub> PL arising from exciton trapping at individual thiol-origami sites. We further demonstrated the technique's versatility by controlling FRET processes in fluorescent dye-origami-MoS<sub>2</sub> hybrid structures. This energy transfer patterning resulted in spatial modulation of MoS<sub>2</sub> PL, achieving a two-fold brightening in dye-to-MoS<sub>2</sub> FRET and quenching in MoS<sub>2</sub>-to-dye FRET. Looking forward, our technique can be used for precise functionalization of a wide range of 2D materials, including TMDs, graphene, and other 2D van der Waals structures. In nanophotonics, our hybrid 2D organic-inorganic structures will enable exciton landscape engineering, where origami can precisely control the number and density of localized defects for next-generation circuits and quantum emitters<sup>54</sup> for quantum communications. Beyond hybrid nanophotonics, our work may find applications in hybrid nanoelectronics,<sup>69</sup> and any heterogeneous fabrication process where molecules or nanoparticles must be integrated with 2D materials with nanoscale precision.

## ACKNOWLEDGMENTS

We thank Philipp Altpeter and Christian Obermayer for assistance in the clean room. I.M. and T.L. acknowledge funding from the ERC consolidator grant “DNA Funs” (Project ID: 818635) T.L. further acknowledges support from the cluster of excellence e-conversion EXC 2089/1- 390776260. This work was funded by the Federal Ministry of Education and Research (BMBF) and the Free State of Bavaria under the Excellence Strategy of the Federal Government and the Länder through the ONE MUNICH Project Munich Multiscale Biofabrication. K.W. and T.T. acknowledge support from the JSPS KAKENHI (Grant Numbers 20H00354 and 23H02052) and World Premier International Research Center Initiative (WPI), MEXT, Japan. A.H. acknowledges funding by the Deutsche Forschungsgemeinschaft (DFG, German Research Foundation) within the Priority Programme SPP 2244 2DMP and the Germany's Excellence Strategy EXC-2111-390814868 (MCQST), as well as by the Bavarian Hightech Agenda within the EQAP project.

## AUTHOR CONTRIBUTIONS STATEMENT

I.M. and A.B. designed this study. I.M. designed, assembled, and purified DNA origami samples, performed DNA origami placement experiments, and conducted AFM measurements and data analysis with assistance from E.E., C.S., and Z.M. Z.L. performed MoS<sub>2</sub> monolayer synthesis and, together with I.M., transferred it onto the origami patterns. K.W. and T.T. performed hBN synthesis. S.Z. performed optical spectroscopy. I.M., A.B., and S.Z. analyzed the data and wrote the manuscript with input from A.H. and T.L.

## COMPETING INTERESTS STATEMENT

The authors declare no competing financial interest.

## FIGURE LEGENDS/CAPTIONS

**Figure 1. DNA origami-programmable organic molecule-MoS<sub>2</sub> hybrid assembly.** (a) Schematic illustration of a DNA origami triangle positioned on a hydrophilic, hydroxyl group covered binding site (green) on a hydrophobic, methyl group covered surface of Si/SiO<sub>2</sub> chip. DNA origami triangle bears 54 adenine “anchor” strands each 21 nt long for on-surface annealing with 19 nt thymine strands bearing a single functional molecule. (b) Schematic illustration of a molecule-origami-MoS<sub>2</sub> assembly. (c) The various steps of the fabrication process of a molecule-origami-MoS<sub>2</sub> assembly. (d) Liquid mode AFM image of DNA origami triangle in the folding buffer. (e) AFM image of a dried Si/SiO<sub>2</sub> chip with the DNA origami triangles positioned onto ~ 120 nm triangular binding sites in a 20 μm-square array with a 250 nm period, fabricated using electron beam lithography. (f) Bright-field microscopy image of the MoS<sub>2</sub> flake on adhesive polycarbonate stamp before transferring onto an origami pattern. (g) Bright-field microscopy image of the MoS<sub>2</sub> flake transferred onto the origami pattern. The scale bar in panel (d) is 50 nm, in panel (e) is 500 nm, and in panels (f) and (g) is 30 μm.

**Figure 2. DNA-programmable exciton landscape in MoS<sub>2</sub> flake on top of the thiol-origami pattern.** (a) Schematic of the patterned area. The nanopatterned area is 20 μm x 25 μm and consists of arrays of triangular binding sites with a size of 120 nm in a square lattice with periods ranging from 1000 nm to 170 nm. (b, c) Free exciton and localized exciton PL intensity maps, measured at 1.88 eV and 1.83 eV, respectively. (d) Representative room-temperature PL spectra of every “step” in the gradient pattern presented in Fig. 2a. (e) Map of localized/free exciton PL peaks ratio, corresponding to the marked area in panel c. Each white triangle indicates the position of a DNA origami triangle. (f) Schematic illustration of the exciton localization scheme in thiol-origami-MoS<sub>2</sub>. (g) Low-temperature PL spectrum from the spot indicated by the red circle in panel (e). (h) Correlation function of localized defect state marked by gray bar in panel (g) with second order coherence at zero time delay  $g^{(2)}(0) = 0.31$ . Scale bar: 4 μm (panels a, b, and c).

**Figure 3. DNA-programmable enhancement of PL of MoS<sub>2</sub>.** (a) Room-temperature absorption (thin lines) and PL spectra (thick lines) of the MoS<sub>2</sub> flake and of the ATTO633 dye in PBS. A and B indicate the MoS<sub>2</sub> exciton bands. (b) Bright-field microscopy image of the MoS<sub>2</sub> flake transferred on top of the ATTO633-origami pattern. (c) Schematic illustration of energy transfer scheme between ATTO633 dye and MoS<sub>2</sub>. (d) Room-temperature PL map of the MoS<sub>2</sub> flake on top of the ATTO633-origami pattern. PL excitation energy is 2.36 eV (525 nm) where the ATTO633 dye has negligible absorption. (e) Room-temperature PL map of the MoS<sub>2</sub> flake on top of the ATTO633-origami pattern. PL excitation energy was 2.21 eV (560 nm) where both MoS<sub>2</sub> and ATTO633 dye absorb light. (f) Room-temperature PL spectra of ATTO633-origami-MoS<sub>2</sub> hybrid assembly (orange curve) and MoS<sub>2</sub> flake alone (violet curve). Inset shows the corresponding normalized PL spectra. Scale bars in (b), (d) and (f) are 10 μm.

## REFERENCES

1. Novoselov KS, Jiang D, Schedin F, Booth TJ, Khotkevich VV, Morozov SV, *et al.* Two-dimensional atomic crystals. *Proceedings of the National Academy of Sciences* 2005, **102**(30): 10451-10453.

2. Wang QH, Kalantar-Zadeh K, Kis A, Coleman JN, Strano MS. Electronics and optoelectronics of two-dimensional transition metal dichalcogenides. *Nature Nanotechnology* 2012, **7**(11): 699-712.
3. Huang Y, Zheng W, Qiu Y, Hu P. Effects of Organic Molecules with Different Structures and Absorption Bandwidth on Modulating Photoresponse of MoS<sub>2</sub> Photodetector. *ACS Applied Materials & Interfaces* 2016, **8**(35): 23362-23370.
4. Huang Y, Zhuge F, Hou J, Lv L, Luo P, Zhou N, *et al.* Van der Waals Coupled Organic Molecules with Monolayer MoS<sub>2</sub> for Fast Response Photodetectors with Gate-Tunable Responsivity. *ACS nano* 2018, **12**(4): 4062-4073.
5. Jariwala D, Howell SL, Chen K-S, Kang J, Sangwan VK, Filippone SA, *et al.* Hybrid, Gate-Tunable, van der Waals p–n Heterojunctions from Pentacene and MoS<sub>2</sub>. *Nano Lett* 2016, **16**(1): 497-503.
6. Chen R, Lin C, Yu H, Tang Y, Song C, Yuwen L, *et al.* Templating C60 on MoS<sub>2</sub> Nanosheets for 2D Hybrid van der Waals p–n Nanoheterojunctions. *Chem Mater* 2016, **28**(12): 4300-4306.
7. Bettis Homan S, Sangwan VK, Balla I, Bergeron H, Weiss EA, Hersam MC. Ultrafast Exciton Dissociation and Long-Lived Charge Separation in a Photovoltaic Pentacene–MoS<sub>2</sub> van der Waals Heterojunction. *Nano Lett* 2017, **17**(1): 164-169.
8. Kim J-S, Yoo H-W, Choi HO, Jung H-T. Tunable Volatile Organic Compounds Sensor by Using Thiolated Ligand Conjugation on MoS<sub>2</sub>. *Nano Lett* 2014, **14**(10): 5941-5947.
9. Li BL, Luo HQ, Lei JL, Li NB. Hemin-functionalized MoS<sub>2</sub> nanosheets: enhanced peroxidase-like catalytic activity with a steady state in aqueous solution. *RSC Advances* 2014, **4**(46): 24256-24262.
10. Zhu T, Yuan L, Zhao Y, Zhou M, Wan Y, Mei J, *et al.* Highly mobile charge-transfer excitons in two-dimensional WS<sub>2</sub>/tetracene heterostructures. *Science Advances* 2018, **4**(1): eaao3104.
11. Thompson JJP, Gerhard M, Witte G, Malic E. Optical signatures of Förster-induced energy transfer in organic/TMD heterostructures. *npj 2D Materials and Applications* 2023, **7**(1): 69.
12. Amani M, Lien D-H, Kiriya D, Xiao J, Azcatl A, Noh J, *et al.* Near-unity photoluminescence quantum yield in MoS<sub>2</sub>. *Science* 2015, **350**(6264): 1065-1068.
13. Wang S, Yang X, Hou L, Cui X, Zheng X, Zheng J. Organic covalent modification to improve thermoelectric properties of TaS<sub>2</sub>. *Nature Communications* 2022, **13**(1): 4401.
14. Varade V, Haider G, Slobodeniuk A, Korytar R, Novotny T, Holy V, *et al.* Chiral Light Emission from a Hybrid Magnetic Molecule–Monolayer Transition Metal Dichalcogenide Heterostructure. *ACS nano* 2023, **17**(3): 2170-2181.
15. Schmidt H, Giustiniano F, Eda G. Electronic transport properties of transition metal dichalcogenide field-effect devices: surface and interface effects. *Chem Soc Rev* 2015, **44**(21): 7715-7736.

16. Chen X, Bartlam C, Lloret V, Moses Badlyan N, Wolff S, Gillen R, *et al.* Covalent Bisfunctionalization of Two-Dimensional Molybdenum Disulfide. *Angew Chem Int Ed* 2021, **60**(24): 13484-13492.
17. Wei T, Al-Fogra S, Hauke F, Hirsch A. Direct Laser Writing on Graphene with Unprecedented Efficiency of Covalent Two-Dimensional Functionalization. *J Am Chem Soc* 2020, **142**(52): 21926-21931.
18. Kollipara PS, Li J, Zheng Y. Optical Patterning of Two-Dimensional Materials. *Research* 2020, **2020**.
19. Tan X, Wang S, Zhang Q, He J, Chen S, Qu Y, *et al.* Laser doping of 2D material for precise energy band design. *Nanoscale* 2023, **15**(21): 9297-9303.
20. Goronzy DP, Ebrahimi M, Rosei F, Arramel, Fang Y, De Feyter S, *et al.* Supramolecular Assemblies on Surfaces: Nanopatterning, Functionality, and Reactivity. *ACS nano* 2018, **12**(8): 7445-7481.
21. Heinrich AJ, Lutz CP, Gupta JA, Eigler DM. Molecule Cascades. *Science* 2002, **298**(5597): 1381-1387.
22. Kocić N, Blank D, Abufager P, Lorente N, Decurtins S, Liu S-X, *et al.* Implementing Functionality in Molecular Self-Assembled Monolayers. *Nano Lett* 2019, **19**(5): 2750-2757.
23. Tsai H-Z, Lischner J, Omrani AA, Liou F, Aikawa AS, Karrasch C, *et al.* A molecular shift register made using tunable charge patterns in one-dimensional molecular arrays on graphene. *Nature Electronics* 2020, **3**(10): 598-603.
24. Rothmund PWK. Folding DNA to create nanoscale shapes and patterns. *Nature* 2006, **440**(7082): 297-302.
25. Douglas SM, Dietz H, Liedl T, Högberg B, Graf F, Shih WM. Self-assembly of DNA into nanoscale three-dimensional shapes. *Nature* 2009, **459**(7245): 414-418.
26. Seeman NC. DNA in a material world. *Nature* 2003, **421**(6921): 427-431.
27. Yan H, Park SH, Finkelstein G, Reif JH, LaBean TH. DNA-templated self-assembly of protein arrays and highly conductive nanowires. *Science* 2003, **301**(5641): 1882-1884.
28. Aldaye FA, Palmer AL, Sleiman HF. Assembling materials with DNA as the guide. *Science* 2008, **321**(5897): 1795-1799.
29. Wang P, Huh J-H, Lee J, Kim K, Park KJ, Lee S, *et al.* Magnetic Plasmon Networks Programmed by Molecular Self-Assembly. *Adv Mater* 2019, **31**(29): 1901364.
30. Liu X, Zhang F, Jing X, Pan M, Liu P, Li W, *et al.* Complex silica composite nanomaterials templated with DNA origami. *Nature* 2018, **559**(7715): 593-598.
31. Sun W, Boulais E, Hakobyan Y, Wang WL, Guan A, Bathe M, *et al.* Casting inorganic structures with DNA molds. *Science* 2014, **346**(6210): 1258361.

32. Kolbeck PJ, Dass M, Martynenko IV, van Dijk-Moes RJ, Brouwer KJ, van Blaaderen A, *et al.* A DNA origami fiducial for accurate 3D AFM imaging. *bioRxiv* 2022.
33. Maune HT, Han S-p, Barish RD, Bockrath M, Iii WAG, Rothemund PWK, *et al.* Self-assembly of carbon nanotubes into two-dimensional geometries using DNA origami templates. *Nature Nanotechnology* 2010, **5**(1): 61-66.
34. Kuzyk A, Schreiber R, Fan Z, Pardatscher G, Roller E-M, Högele A, *et al.* DNA-based self-assembly of chiral plasmonic nanostructures with tailored optical response. *Nature* 2012, **483**(7389): 311-314.
35. Voigt NV, Tørring T, Rotaru A, Jacobsen MF, Ravnsbæk JB, Subramani R, *et al.* Single-molecule chemical reactions on DNA origami. *Nature Nanotechnology* 2010, **5**(3): 200-203.
36. Knudsen JB, Liu L, Bank Kodal AL, Madsen M, Li Q, Song J, *et al.* Routing of individual polymers in designed patterns. *Nature Nanotechnology* 2015, **10**(10): 892-898.
37. Hartl C, Frank K, Amenitsch H, Fischer S, Liedl T, Nickel B. Position Accuracy of Gold Nanoparticles on DNA Origami Structures Studied with Small-Angle X-ray Scattering. *Nano Lett* 2018, **18**(4): 2609-2615.
38. Funke JJ, Dietz H. Placing molecules with Bohr radius resolution using DNA origami. *Nature Nanotechnology* 2016, **11**(1): 47-52.
39. Kershner RJ, Bozano LD, Micheel CM, Hung AM, Fornof AR, Cha JN, *et al.* Placement and orientation of individual DNA shapes on lithographically patterned surfaces. *Nature Nanotechnology* 2009, **4**(9): 557-561.
40. Hung AM, Micheel CM, Bozano LD, Osterbur LW, Wallraff GM, Cha JN. Large-area spatially ordered arrays of gold nanoparticles directed by lithographically confined DNA origami. *Nature Nanotechnology* 2010, **5**(2): 121-126.
41. Sikeler C, Haslinger F, Martynenko IV, Liedl T. DNA Origami-Directed Self-Assembly of Gold Nanospheres for Plasmonic Metasurfaces. *Adv Funct Mater* 2024, **34**(42): 2404766.
42. Martynenko IV, Erber E, Ruider V, Dass M, Posnjak G, Yin X, *et al.* Site-directed placement of three-dimensional DNA origami. *Nat Nanotechnol* 2023, **18**(12): 1456-1462.
43. Gopinath A, Miyazono E, Faraon A, Rothemund PWK. Engineering and mapping nanocavity emission via precision placement of DNA origami. *Nature* 2016, **535**(7612): 401-405.
44. Gopinath A, Thachuk C, Mitskovets A, Atwater HA, Kirkpatrick D, Rothemund PWK. Absolute and arbitrary orientation of single-molecule shapes. *Science* 2021, **371**(6531): eabd6179.
45. Douglas SM, Marblestone AH, Teerapittayanon S, Vazquez A, Church GM, Shih WM. Rapid prototyping of 3D DNA-origami shapes with caDNAno. *Nucleic Acids Res* 2009, **37**(15): 5001-5006.
46. Kim D-N, Kilchherr F, Dietz H, Bathe M. Quantitative prediction of 3D solution shape and flexibility of nucleic acid nanostructures. *Nucleic Acids Res* 2011, **40**(7): 2862-2868.

47. Gopinath A, Rothmund PWK. Optimized Assembly and Covalent Coupling of Single-Molecule DNA Origami Nanoarrays. *ACS nano* 2014, **8**(12): 12030-12040.
48. Kirubasankar B, Won YS, Adofo LA, Choi SH, Kim SM, Kim KK. Atomic and structural modifications of two-dimensional transition metal dichalcogenides for various advanced applications. *Chem Sci* 2022, **13**(26): 7707-7738.
49. Mouri S, Miyauchi Y, Matsuda K. Tunable Photoluminescence of Monolayer MoS<sub>2</sub> via Chemical Doping. *Nano Lett* 2013, **13**(12): 5944-5948.
50. Sim DM, Kim M, Yim S, Choi M-J, Choi J, Yoo S, *et al.* Controlled Doping of Vacancy-Containing Few-Layer MoS<sub>2</sub> via Highly Stable Thiol-Based Molecular Chemisorption. *ACS nano* 2015, **9**(12): 12115-12123.
51. Mak KF, Lee C, Hone J, Shan J, Heinz TF. Atomically Thin  $\text{MoS}_2$ : A New Direct-Gap Semiconductor. *Phys Rev Lett* 2010, **105**(13): 136805.
52. Neumann A, Lindlau J, Nutz M, Mohite AD, Yamaguchi H, Högele A. Signatures of defect-localized charged excitons in the photoluminescence of monolayer molybdenum disulfide. *Physical Review Materials* 2018, **2**(12): 124003.
53. Mitterreiter E, Schuler B, Micevic A, Hernangómez-Pérez D, Barthelmi K, Cochrane KA, *et al.* The role of chalcogen vacancies for atomic defect emission in MoS<sub>2</sub>. *Nature Communications* 2021, **12**(1): 3822.
54. Klein J, Lorke M, Florian M, Sigger F, Sigl L, Rey S, *et al.* Site-selectively generated photon emitters in monolayer MoS<sub>2</sub> via local helium ion irradiation. *Nature Communications* 2019, **10**(1): 2755.
55. Liu S, Liu Y, Holtzman L, Li B, Holbrook M, Pack J, *et al.* Two-Step Flux Synthesis of Ultrapure Transition-Metal Dichalcogenides. *ACS nano* 2023, **17**(17): 16587-16596.
56. Tonndorf P, Schmidt R, Schneider R, Kern J, Buscema M, Steele GA, *et al.* Single-photon emission from localized excitons in an atomically thin semiconductor. *Optica* 2015, **2**(4): 347-352.
57. Srivastava A, Sidler M, Allain AV, Lembke DS, Kis A, Imamoglu A. Optically active quantum dots in monolayer WSe<sub>2</sub>. *Nature Nanotechnology* 2015, **10**(6): 491-496.
58. He Y-M, Clark G, Schaibley JR, He Y, Chen M-C, Wei Y-J, *et al.* Single quantum emitters in monolayer semiconductors. *Nature Nanotechnology* 2015, **10**(6): 497-502.
59. Koperski M, Nogajewski K, Arora A, Cherkez V, Mallet P, Veuillen JY, *et al.* Single photon emitters in exfoliated WSe<sub>2</sub> structures. *Nature Nanotechnology* 2015, **10**(6): 503-506.
60. Chakraborty C, Kinnischtzke L, Goodfellow KM, Beams R, Vamivakas AN. Voltage-controlled quantum light from an atomically thin semiconductor. *Nature Nanotechnology* 2015, **10**(6): 507-511.

61. Christopher JW, Goldberg BB, Swan AK. Long tailed trions in monolayer MoS<sub>2</sub>: Temperature dependent asymmetry and resulting red-shift of trion photoluminescence spectra. *Sci Rep* 2017, **7**(1): 14062.
62. Tongay S, Zhou J, Ataca C, Lo K, Matthews TS, Li J, *et al.* Thermally Driven Crossover from Indirect toward Direct Bandgap in 2D Semiconductors: MoSe<sub>2</sub> versus MoS<sub>2</sub>. *Nano Lett* 2012, **12**(11): 5576-5580.
63. He X, Htoon H, Doorn SK, Pernice WHP, Pyatkov F, Krupke R, *et al.* Carbon nanotubes as emerging quantum-light sources. *Nature Materials* 2018, **17**(8): 663-670.
64. Li X, Jones AC, Choi J, Zhao H, Chandrasekaran V, Pettes MT, *et al.* Proximity-induced chiral quantum light generation in strain-engineered WSe<sub>2</sub>/NiPS<sub>3</sub> heterostructures. *Nature Materials* 2023, **22**(11): 1311-1316.
65. Hu Z, Krisnanda T, Fieramosca A, Zhao J, Sun Q, Chen Y, *et al.* Energy transfer driven brightening of MoS<sub>2</sub> by ultrafast polariton relaxation in microcavity MoS<sub>2</sub>/hBN/WS<sub>2</sub> heterostructures. *Nature Communications* 2024, **15**(1): 1747.
66. Swathi RS, Sebastian KL. Resonance energy transfer from a dye molecule to graphene. *The Journal of Chemical Physics* 2008, **129**(5).
67. Hernández-Martínez PL, Govorov AO, Demir HV. Generalized Theory of Förster-Type Nonradiative Energy Transfer in Nanostructures with Mixed Dimensionality. *J Phys Chem C* 2013, **117**(19): 10203-10212.
68. Baimuratov AS, Högele A. Valley-selective energy transfer between quantum dots in atomically thin semiconductors. *Sci Rep* 2020, **10**(1): 16971.
69. Markeev PA, Najafidehaghani E, Samu GF, Sarosi K, Kalkan SB, Gan Z, *et al.* Exciton Dynamics in MoS<sub>2</sub>-Pentacene and WSe<sub>2</sub>-Pentacene Heterojunctions. *ACS nano* 2022, **16**(10): 16668-16676.
70. Bilgin I, Raeliarijaona AS, Lucking MC, Hodge SC, Mohite AD, de Luna Bugallo A, *et al.* Resonant Raman and Exciton Coupling in High-Quality Single Crystals of Atomically Thin Molybdenum Diselenide Grown by Vapor-Phase Chalcogenization. *ACS nano* 2018, **12**(1): 740-750.
71. Pizzocchero F, Gammelgaard L, Jessen BS, Caridad JM, Wang L, Hone J, *et al.* The hot pick-up technique for batch assembly of van der Waals heterostructures. *Nature Communications* 2016, **7**(1): 11894.

## METHODS

### DNA Origami design, preparation and purification

The 'sameside sharp triangle' design is adapted from Ref.<sup>1</sup> We modified 54 staples from the original design by extending them with 21-nucleotide adenine extensions on the 3' end. The positions of these extended staples are shown in Supplementary Fig. S1. These 21-nucleotide adenine-extended staples serve as linkers that bind to a 19-nucleotide thymine strand bearing a single functional molecule on its 5' end (either an ATTO633 dye, an ATTORho101 dye, or a thiol group) in a 'shear' configuration.

DNA origami triangles were folded by mixing scaffold strands (7249 nucleotides long M13mp18 single-stranded DNA) with an excess of staple strands in folding buffer (10 mM Tris, 1 mM EDTA, 12.5 mM MgCl<sub>2</sub>, pH 8.35). The scaffold DNA was mixed with all staples except for 54 staples, which were replaced with modified versions containing 21-nucleotide adenine extensions at the 3' ends (IDT Technologies, 200 μM). The final concentrations in the folding buffer were: 20 nM scaffold strand, 100 nM staple strands, and 2000 nM polyA-modified staples (IDT Technologies, 200 μM). The samples were annealed in a PCR machine (Biometra TRIO Thermal Cycler, Analytik Jena) and purified from excess staples by Amicon filtration as described in Ref.<sup>42</sup> After Amicon purification, the concentration of triangles typically ranged from 70 to 100 nM, with a recovery yield of 40-50%. Scaffold strands were produced from M13 phage replication in *Escherichia coli*. All chemicals were obtained from Sigma Aldrich unless otherwise stated.

#### Preparation of the substrates and DNA origami placement

Si/SiO<sub>2</sub> substrates were patterned using electron-beam lithography, following protocols from Ref.<sup>2</sup> with slight modifications. A 4-inch Si/SiO<sub>2</sub> wafer with a 100 nm thermal oxide layer (Microchemicals) was diced into 1 cm × 1 cm chips. Clean chips were primed with 10 mL of hexamethyldisilazane (HMDS) in a 4 L desiccator. The priming time was optimized to maintain a Si/SiO<sub>2</sub> surface contact angle of 70°-75° after HMDS deposition. Triangular binding sites, where individual DNA triangles would bind, were patterned into poly(methyl methacrylate) resist by electron-beam lithography. Similarly, we patterned approximately 1-μm lines to which multiple origami would bind at random positions and orientations. The chips were then developed with a 1:3 solution of methyl isobutyl ketone (MIBK) and isopropanol (IPA). The HMDS in the developed areas was removed using O<sub>2</sub> plasma for 6 seconds in a plasma cleaner (PICO). The resist was stripped by ultrasonication in N-methyl pyrrolidone (NMP) at 50°C for 30 minutes. The substrates were briefly rinsed with 2-propanol, dried in a nitrogen stream, and used immediately.

DNA triangles were bound to the patterned substrates as previously described in Refs.<sup>42, 47</sup> A 20-60 μL drop of freshly folded and purified DNA origami was deposited onto the surface of the chips in placement buffer (5 mM Tris, 35 mM MgCl<sub>2</sub>, pH 8.35). After incubation for 1 hour at RT in a 100% humidity incubator, excess DNA origami was removed from the surface by performing eight buffer replacement steps and purifying with 0.1% Tween 20.

#### Post-placement functionalization of DNA origami

After placement, DNA triangles were labelled with functional molecules (either an ATTO633 dye, ATTORho101 dye or a thiol group) and dried using ethanol drying. Labeling was performed by incubating the placed origami, bearing 21-nucleotide adenine extensions, in a placement buffer containing 200 nM of a 19-nucleotide thymine strand bearing a single fluorescent dye (Biomers, HPLC purified, 400 μM) or a thiol group (Biomers, HPLC purified, 100 μM) for 1 hour at room temperature. Excess ssDNA strands were removed from the surface by performing eight buffer replacement steps and purifying with 0.1% Tween 20. After this step, chips with absorbed DNA origami were air-dried using an ethanol dilution series as previously described.<sup>47</sup>

#### MoS<sub>2</sub> monolayer synthesis and transfer

Monolayers of MoS<sub>2</sub> were synthesized by the vapor phase chalcogenization method<sup>70</sup> on thermally oxidized SiO<sub>2</sub>/Si substrates with oxide thickness of 285 nm. A three-zone furnace system (Carbolite Gero) equipped with a 1 inch quartz tube was used for growth under ambient pressure. In order to precisely place MoS<sub>2</sub> monolayers onto molecule-origami patterns, a dry-transfer method with PDMS/PC stamps was used.<sup>71</sup> An hBN flake with a

thickness around 100 nm was firstly picked up at 50 °C, followed by a triangular monolayer MoS<sub>2</sub> at 145 °C. The entire stack was subsequently released from the stamp onto a SiO<sub>2</sub>/Si target substrate with molecule-origami pattern at a temperature of 180°C. The sample was then soaked in chloroform solution for 5 min to remove polycarbonate residues, cleaned by acetone and isopropanol and annealed under ultrahigh vacuum for 12 hours.

#### Characterization techniques and data analysis

UV-vis absorption measurements were performed with a NanoDrop ND-1000 Spectrophotometer (Thermo Scientific). Tapping-mode AFM of dried Si/SiO<sub>2</sub> substrates with triangular DNA origami was carried out on a Dimension ICON AFM (Bruker). OTESPA silicon tips (300 kHz, Veeco Probes) were used for imaging in air. Images are analysed with the Software Gwydion.

Hyperspectral Photoluminescence (PL) imaging was performed using a custom-built scanning confocal microscope. The sample was mounted on piezo-stepping units (ANPxyz101, attocube system) for precise positioning with respect to the confocal spot of an apochromatic objective (LT-APO/532-RAMAN, attocube system). Continuous-wave diode lasers with a power of 2 μW were used for excitation to prevent sample damage. Spectrally sharp short-pass and long-pass filters (Semrock) were employed in the excitation and detection paths, respectively, to eliminate laser light. The sample's PL signal was dispersed by a monochromator (Acton SpectraPro 300i, Roper Scientific) with a 300 grooves/mm grating and detected using a Peltier-cooled charge-coupled device (CCD, Andor iDus 416). We subtracted the hBN background emission from the raw PL data.

The low-temperature PL measurements were performed in a close-cycle cryostat (attoDRY800, attocube system) with a base temperature of 4 K, using the same scanning confocal microscope as for the room-temperature measurements. The second-order photon-correlation  $g^{(2)}(\tau)$  measurements were carried out using a standard Hanbury–Brown and Twiss setup. The sample was excited by a supercontinuum laser (SuperK EXTREME, NKT Photonics) tuned to 550nm, and the emission was detected with a pair of silicon avalanche photodiodes ( $\tau$ -SPAD, PicoQuant). Detection events were recorded and correlated with a time-correlated single-photon counting (TCSPC) module (PicoHarp300, PicoQuant).

#### DATA AVAILABILITY

The authors confirm that the data supporting the findings of this study are available within the article and its supplementary materials.

#### METHODS-ONLY REFERENCES

1. Gopinath A, Rothmund PWK. Optimized Assembly and Covalent Coupling of Single-Molecule DNA Origami Nanoarrays. *ACS nano* 2014, **8**(12): 12030-12040.
2. Martynenko IV, Erber E, Ruider V, Dass M, Posnjak G, Yin X, *et al.* Site-directed placement of three-dimensional DNA origami. *Nat Nanotechnol* 2023, **18**(12): 1456-1462.

## **Contents**

Supplementary Notes 1–4

Supplementary Figures 1–7

Additional References

### **Supplementary Note 1. DNA origami “anchors” design**

The ‘sameside sharp triangle’ design is taken from [1]. We modified 54 staples on the inner and outer edges of the triangle by extending them with 21 nt adenine extensions on the 5’ end (see Supplementary Figure 1). These extended strands nearly always point towards the upper side of the surface-bound triangle.

### **Supplementary Note 2. Design of the DNA patterns and AFM characterization**

In this study we employed three distinct patterns for DNA triangle assembly, detailed in Supplementary Figures 2-4.

- Pattern 1: A 25  $\mu\text{m}$  square array of 120 nm triangular binding sites with a 170 nm period (Supplementary Figure 2).

- Pattern 2: A 20  $\mu\text{m}$   $\times$  25  $\mu\text{m}$  pattern featuring square arrays of DNA triangles, with periods gradually decreasing from 1000 nm to 170 nm (Supplementary Figure 3).

- Pattern 3: A 40  $\mu\text{m}$  continuous fractal triangle filling curve with 1  $\mu\text{m}$  line thickness, where multiple DNA triangles bind at random positions and orientations (Supplementary Figure 4).

Following placement, chips containing functionalized DNA triangles were dried and imaged using dry-mode atomic force microscopy (AFM; Dimension ICON AFM, Bruker). Each AFM image was processed using the Gwyddion software [2]. AFM measurements confirmed a DNA layer height of approximately 2 nm across all patterns, consistent with the expected height of a DNA double helix of 2 nm (Supplementary Figures 2-4).

### **Supplementary Note 3. DNA-programmable functionalization of MoS<sub>2</sub> with thiol derivative molecule.**

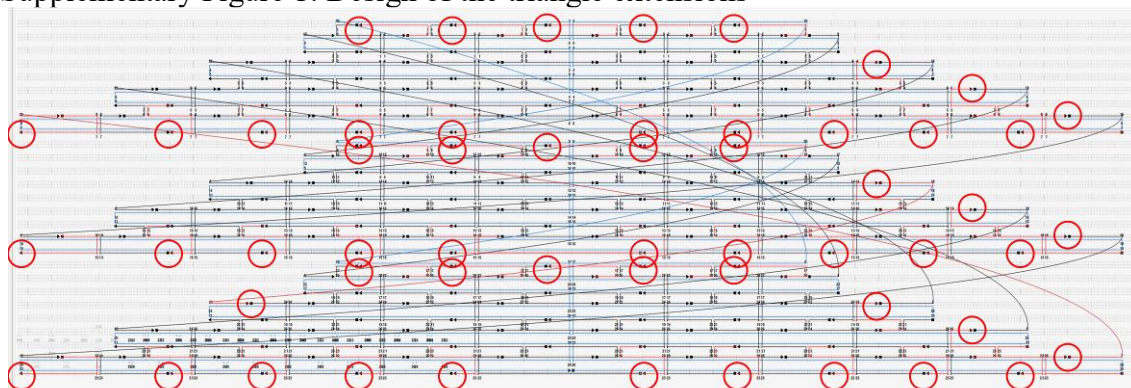
We coupled monolayer MoS<sub>2</sub> to thiolated 19-nt thymine strands, precisely positioned on a large-scale chip pattern via DNA-directed assembly. DNA origami triangles, each functionalized with 54 thiolated 19-nt thymine strands, were organized into 20  $\mu\text{m}$ -square arrays with a 170 nm periodicity, as shown in the AFM image in Supplementary Figure 2. These arrays were subsequently covered with a TMD flake, illustrated in the optical image in Supplementary Figure 5a. The corresponding photoluminescence (PL) map and representative PL spectra of MoS<sub>2</sub> and thiol-origami-MoS<sub>2</sub> are provided in Supplementary Figure 5b and c, respectively. In the thiol-origami region, the MoS<sub>2</sub> exciton A PL exhibited a red shift, indicative of exciton state localization within MoS<sub>2</sub>.

As a control, MoS<sub>2</sub> was transferred onto an origami pattern without the thiolated strands present on the DNA triangles. This reference sample showed no significant changes in the PL of the DNA-MoS<sub>2</sub> pattern.

### **Supplementary Note 4. Photoexcitation energy transfer from the TMD to the dye**

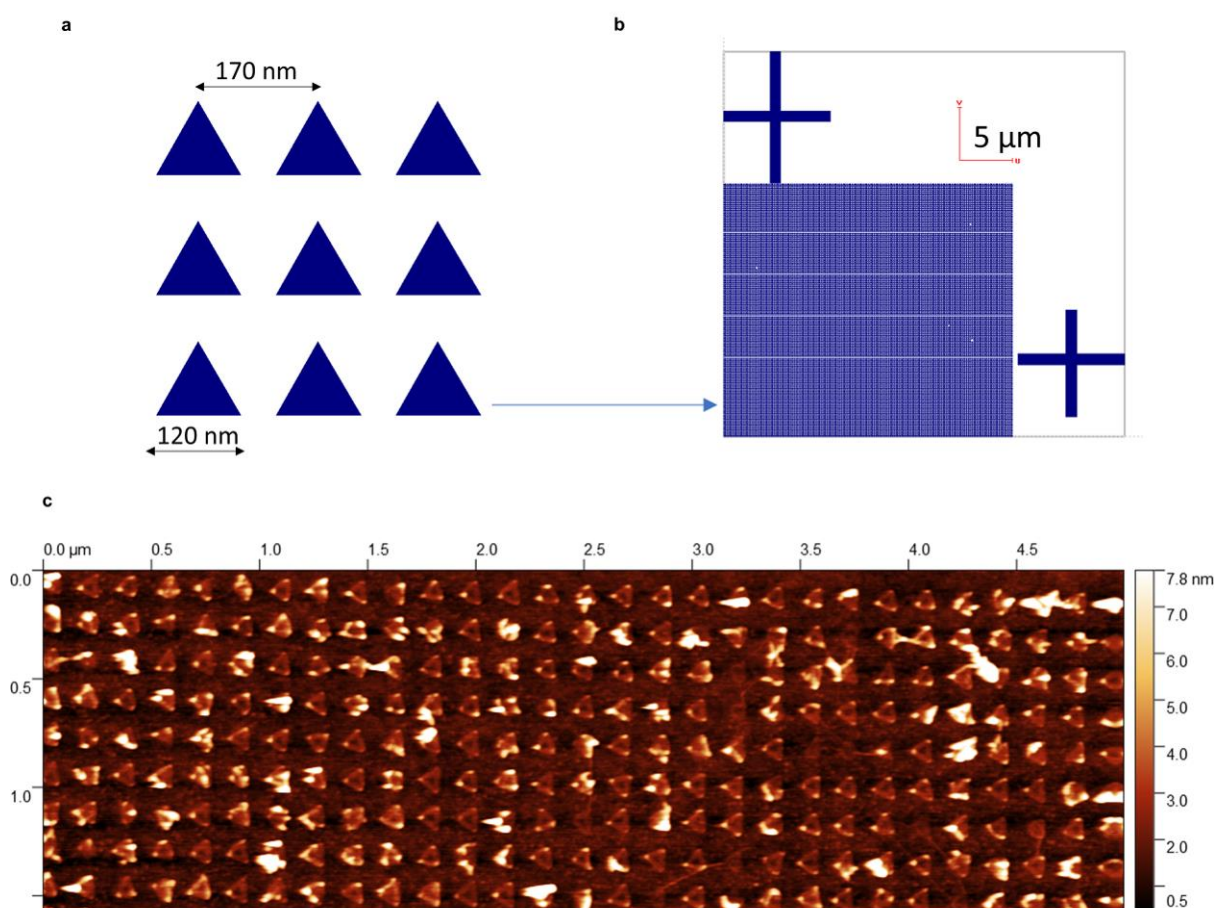
By carefully selecting the energy level of the fluorescent dye, we can facilitate energy transfer from MoS<sub>2</sub> to the dye. For this purpose, we employed ATTORho101 dye, whose energy level of fundamental transition S<sub>0</sub>-S<sub>1</sub> closely aligns with the high-energy B exciton state of MoS<sub>2</sub> (see Supplementary Figure 7a and 7b for the energy level scheme and experimental data). Consequently, MoS<sub>2</sub> transfer photoexcitation energy to the dye, leading to a significant quenching of the MoS<sub>2</sub> PL signal. This quenching is evident when comparing optical images of ATTORho101-origami-MoS<sub>2</sub> hybrid assemblies with the corresponding PL map (Supplementary Figure 6c and 6d). The localized quenching of MoS<sub>2</sub> PL aligns precisely with the underlying ATTORho101-origami pattern. Furthermore, the PL peak of the MoS<sub>2</sub>-ATTORho101-origami hybrid exhibits broadening, characterized by red and blue shoulders, compared to the PL peak of non-patterned MoS<sub>2</sub> (see Supplementary Figure 6e).

### Supplementary Figure 1: Design of the triangle extensions



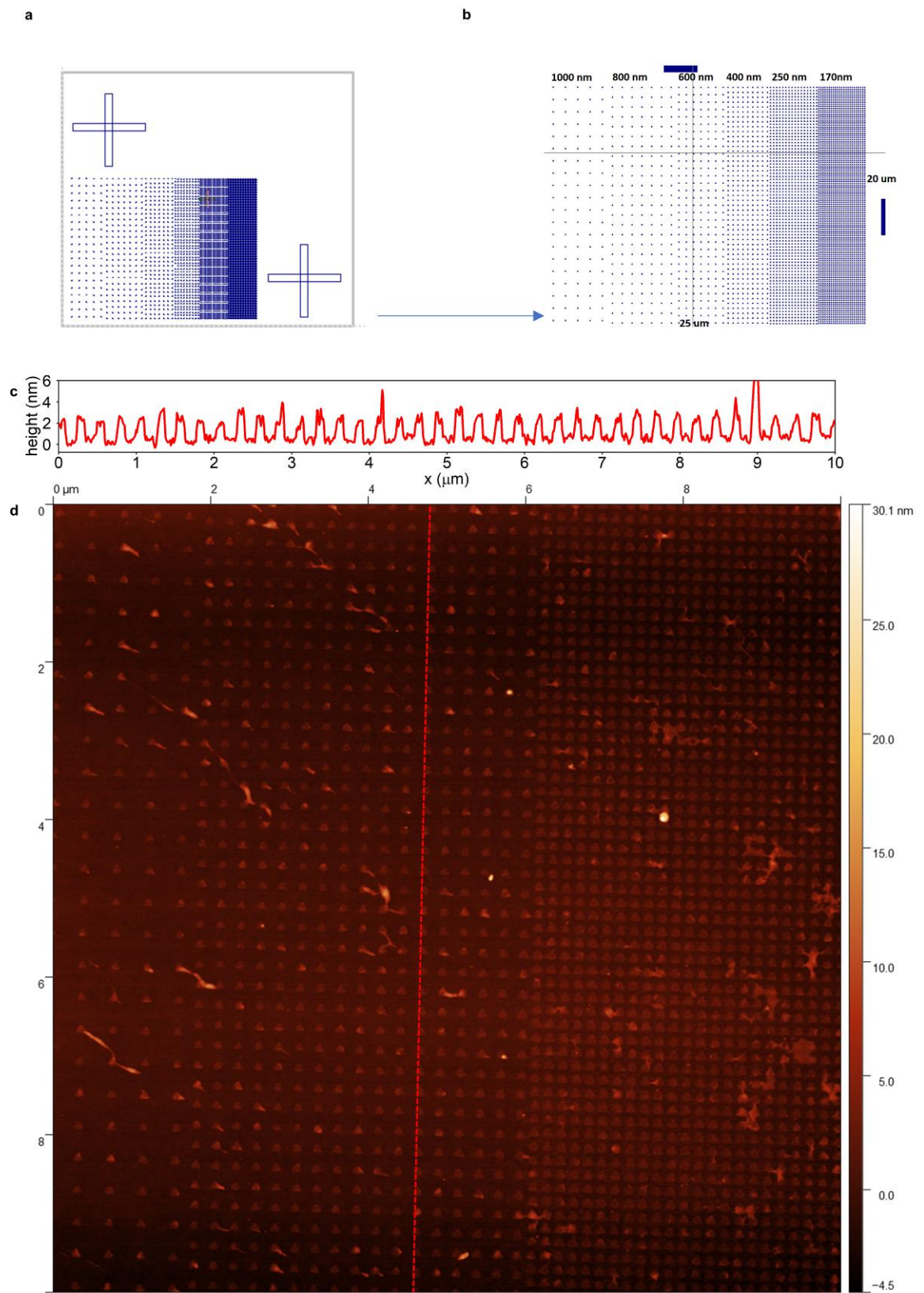
The staple diagrams of the triangle exported from cadnano 2.2.[3] Red circles indicate the 54 staples on the triangle which are extended by 21 adenine nucleotides on the 3' end. These poly(A)- functionalized positions were added by hand as red circles.

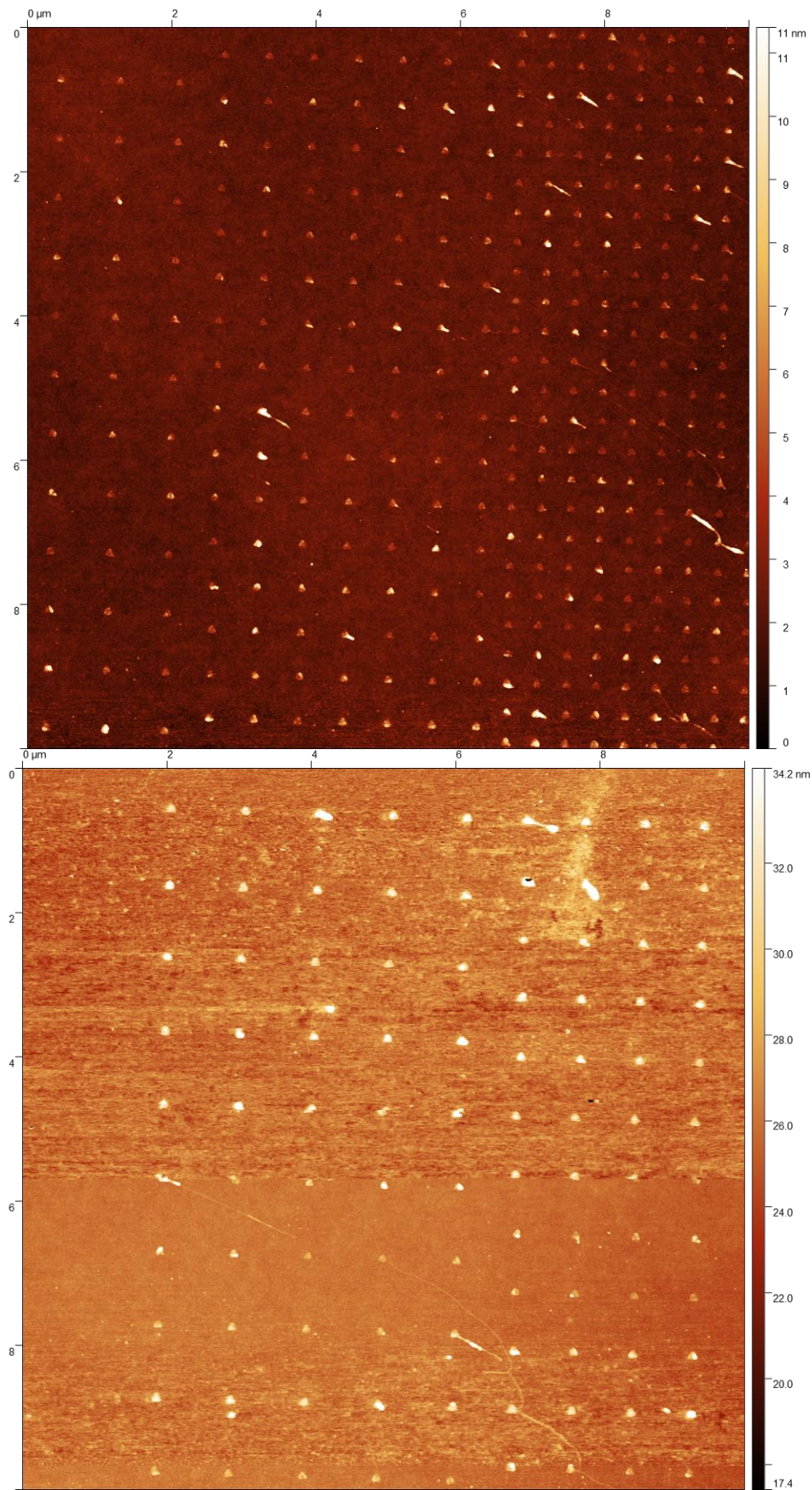
### Supplementary Figure 2: Nanopattern 1 design and AFM characterization



**a, b** Schematic of a patterned area. Crosses are used as fiducial markers. The nanopatterned area is  $25\ \mu\text{m} \times 25\ \mu\text{m}$  and consists of arrays of triangular binding sites with size of  $120\ \text{nm}$  in a square lattice with  $170\ \text{nm}$  period. Panel **a** shows a zoomed-in area of the lattice. **c** Typical dry-mode AFM images of Si/SiO<sub>2</sub> patterned chips with triangles bearing 54 T<sub>19</sub> extensions with  $170\ \text{nm}$  period between triangles. The AFM image size is  $1.5\ \mu\text{m} \times 5\ \mu\text{m}$ .

Supplementary Figure 3: Nanopattern 2 design and AFM characterization

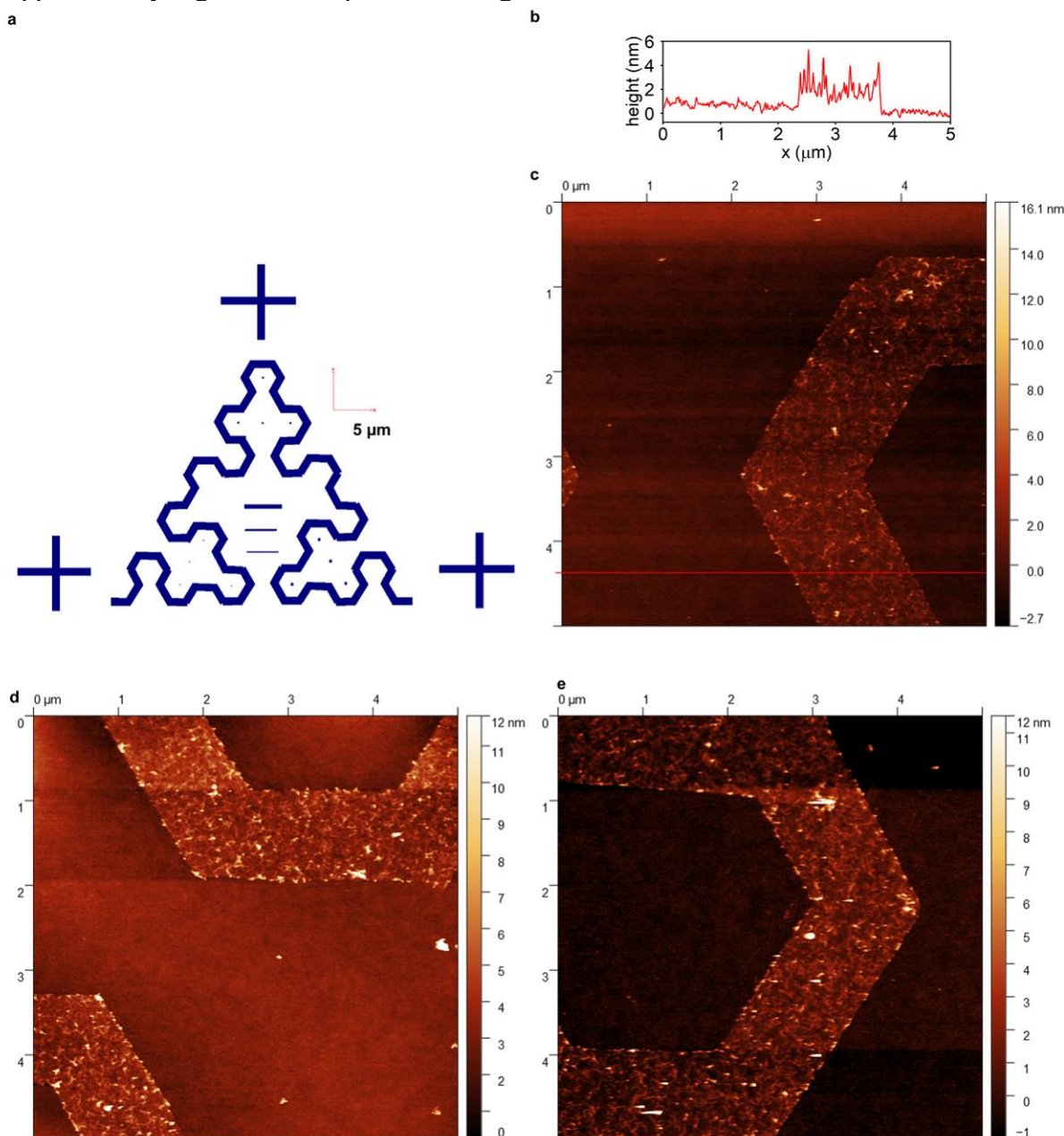




**a, b** Schematic of a patterned area. Crosses are used as fiducial markers. The nanopatterned

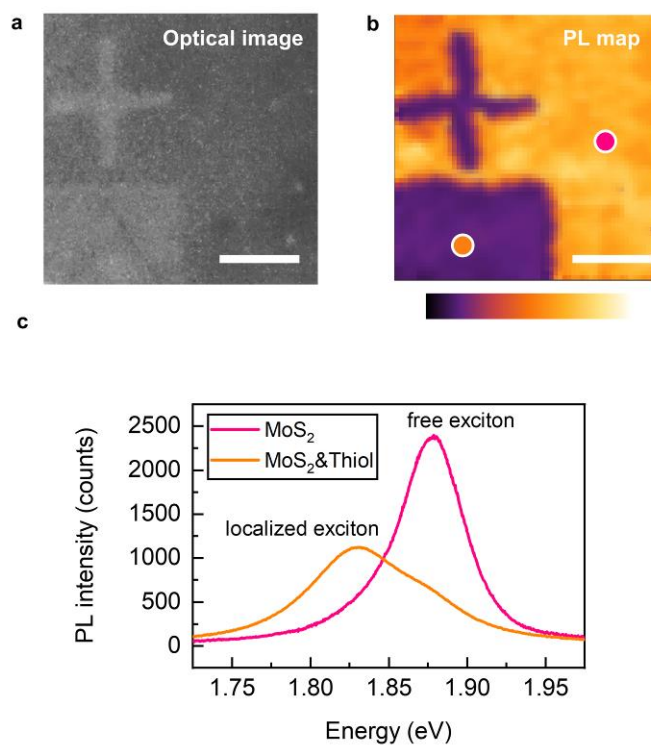
area is  $20\ \mu\text{m} \times 25\ \mu\text{m}$  and consists of arrays of triangular binding sites with size of  $120\ \text{nm}$  in a square lattice with periods gradually decreasing from  $100\ \text{nm}$  to  $170\ \text{nm}$ . **c** Typical height profile from dry-mode AFM images of Si/SiO<sub>2</sub> patterned chips with triangles bearing 54 T<sub>19</sub> extensions with thiol group on its 5' end. **d** Typical dry-mode AFM images of Si/SiO<sub>2</sub> patterned chips with triangles bearing 54 T<sub>19</sub> extensions with thiol group on its 5' end. The AFM images size is  $10\ \mu\text{m} \times 10\ \mu\text{m}$ .

Supplementary Figure 4: Nanopattern 3 design and AFM characterization



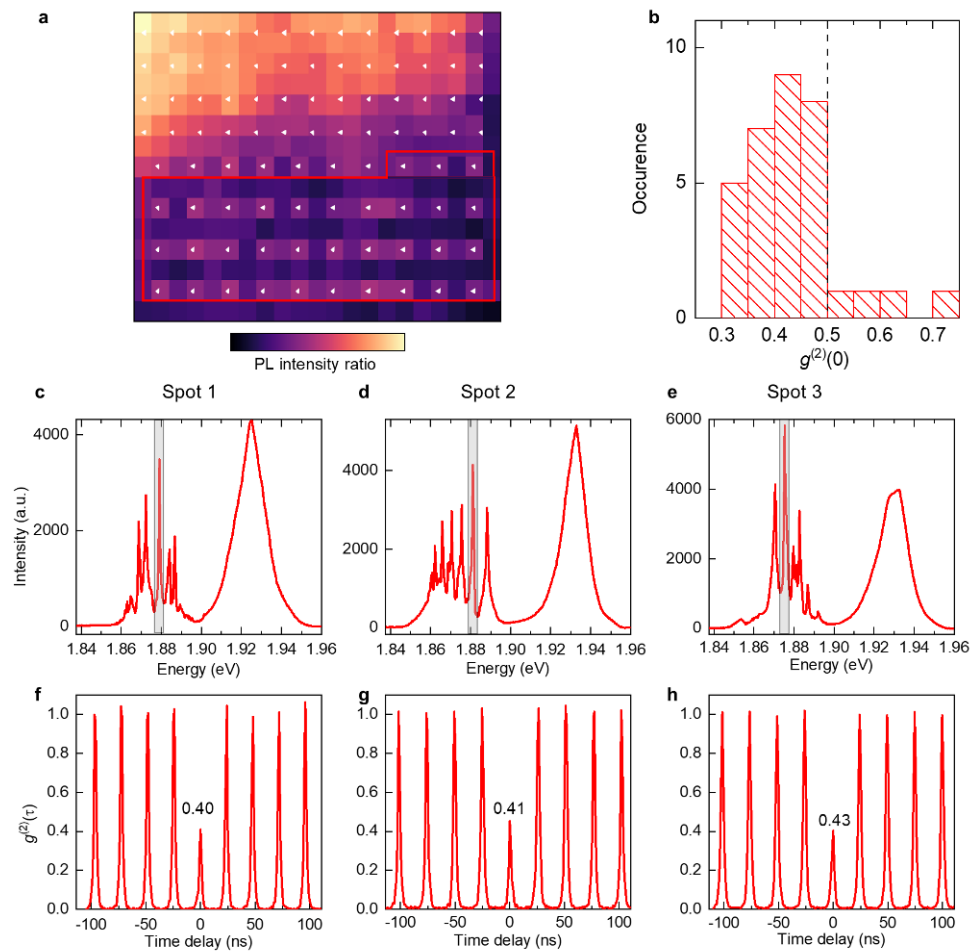
**a** Schematic of a patterned area. Crosses are used as fiducial markers.  $40\ \mu\text{m}$ -sized continuous fractal triangle filling curves with  $1\ \mu\text{m}$  line thickness where multiple origami at random positions and orientations. **c** Typical height profile from dry-mode AFM image of Si/SiO<sub>2</sub> patterned chips with triangles bearing 54 T<sub>19</sub> extensions with single ATTO633 dye molecule on its 5' end. **b-d** Typical dry-mode AFM images of Si/SiO<sub>2</sub> patterned chips with triangles bearing 54 T<sub>19</sub> extensions with single ATTO633 dye molecule on its 5' end. The AFM image size is  $5\ \mu\text{m} \times 5\ \mu\text{m}$ .

Supplementary Figure 5: DNA-programmable thiol functionalization of MoS<sub>2</sub>.



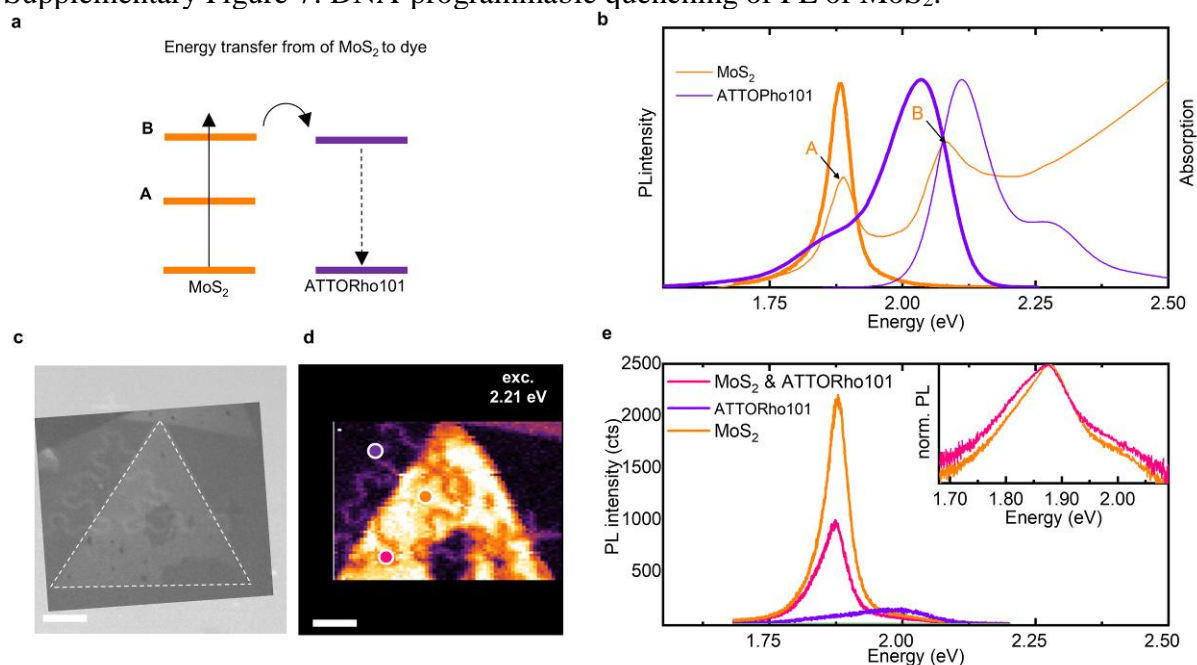
**a** Bright-field microscopy image of the MoS<sub>2</sub> flake transferred on top of the thiol-origami pattern. **b** Room-temperature PL map of the MoS<sub>2</sub> flake on top of the thiol-origami pattern. PL excitation energy is 2.21 eV (560 nm). Room-temperature PL spectra of two different spots of the PL map presented in panel **b**. Pink spot: thiol-origami-MoS<sub>2</sub> hybrid assembly. Orange spot: MoS<sub>2</sub>. (b) Scale bars in **a** and **b** are 4  $\mu$ m.

Supplementary Figure 6: DNA origami-programmable quantum light sources in MoS<sub>2</sub>



**(a)** Map of localized/free exciton PL peaks ratio, corresponding to the marked area in panel **c** in Fig. 2 in the manuscript. Each white triangle indicates the position of a DNA origami triangle. **(b)** A statistical histogram shows the second-order coherence at zero-time delay, measured at 33 spots, each corresponding to the position of a DNA origami triangle bearing 54 T19 extensions with thiol group on its 5' end. These 33 measured spots are marked by red line in panel (a). **(c, d, e)** Low temperature 4K PL spectra from the three measured spots. **(f, g, h)** Correlation functions of the localized defect states indicated by the gray bars in panels (c), (d), and (e). The values of the second order coherence at zero time delay,  $g^{(2)}(0)$ , are indicated in each correlation function plot.

Supplementary Figure 7: DNA-programmable quenching of PL of MoS<sub>2</sub>.



**a** Schematic illustration of energy transfer scheme between MoS<sub>2</sub> and ATTORho101. **b** Room-temperature absorption (thin lines) and PL spectra (thick lines) of MoS<sub>2</sub> flake and ATTORho101 dye in phosphate-buffered saline (PBS). **c** Bright-field microscopy image of the MoS<sub>2</sub> flake transferred on top of the ATTORho101-origami pattern. **d** Room-temperature PL map of the MoS<sub>2</sub> flake on top of the ATTORho101-origami. PL excitation energy is 2.21 eV (560 nm). **e** Room-temperature PL spectra of three different spots of the PL map presented in panel **d**. Pink spot: ATTORho101-origami-MoS<sub>2</sub> hybrid assembly. Violet spot: ATTORho101-origami. Orange spot: non-patterned MoS<sub>2</sub> flake. Scale bars in (c), (d) are 10  $\mu$ m.

### **Additional References**

- [1] A. Gopinath, P.W.K. Rothmund, ACS nano, 8 (2014) 12030-12040.
- [2] D. Nečas, P. Klapetek, Central European Journal of Physics, 10 (2012) 181-188.
- [3] S.M. Douglas, A.H. Marblestone, S. Teerapittayanon, A. Vazquez, G.M. Church, W.M. Shih, Nucleic Acids Res., 37 (2009) 5001-5006.